

The 3D Transition to Turbulence in a Circular Cylinder Wake by Means of Direct Numerical Simulation (18pt, Times)

Line-spacings : From title up to authors line:24pt. From authors line to end of affiliation lines: 16pt

Marianna BRAZA, author2, author3, ... (12pt, Times, Bold)

Institut de Mécanique des Fluides de Toulouse, Unité Mixte C.N.R.S.-I.N.P.T. 5502,

Av. du Prof. Camille Soula, 31400 Toulouse, France, email of the corresponding author (italic, 10pt, Times)

Line-spacing : Between: end of affiliation lines to end of key-words : 15pt

Abstract. (11pt, times new roman, bold) The three-dimensional transition to turbulence in the flow around a circular cylinder has been analysed physically by performing direct numerical simulation to solve the system of Navier-Stokes equations. Etc..., etc... The wavelengths of these undulations have been determined *versus* Reynolds number. As this parameter increases, ... is evaluated by the present DNS approach in association with the Ginzburg-Landau model. Therefore, the linear and non-linear parts of the flow transition have been quantified by means of the amplitude evolution *versus* time obtained by the present DNS, in conjunction with the mentioned global oscillator model.

Key words: instability, transition, DNS, bluff-bodies, wings, incompressible flow.

Line-spacing : Between:Key-words and full text: 15pt

1. Introduction (Times New Roman 13pt, Bold)

Leave one line. First line after each heading starts flush left. First line of a new paragraph starts at 6mm

Concerning (times new roman, 13pt) the flow around a circular cylinder, fascinating phenomena occur in respect to the three-dimensionality of originally 2D vortex structures, as Reynolds number increases. Previous studies have reported that this first step to transition is essentially two-dimensional [7, 27], following a Hopf bifurcation, also known as a Poincaré-Andronov bifurcation [33]. The critical Reynolds number (order of 47) had been accurately evaluated by the Stuart-Landau global oscillator model, on the basis of the physical experiment by Provansal et al. [34], as well as by continuation methods using the steady-state approach near the threshold [19]. By performing three-dimensional simulations of the flow past the cylinder in the Reynolds number range (100-300) it has been quantified that this flow pattern remains essentially two-dimensional up to Reynolds number of order 180 as shown by Persillon and Braza [28], [30]. etc..., etc...

of transition are analysed in detail, in the present study.

Line-spacing : 15pt Leave two lines between end of paragraph and beginning of next section

2. 3D Transition Features in Incompressible Wakes

Line-spacing : Full text : 15pt

The Navier-Stokes equations for an incompressible viscous fluid past a circular cylinder are solved in a general curvilinear coordinates system normalised by the

cylinder's diameter D and the uniform upstream velocity. The pressure-velocity formulation is used as well as a predictor-corrector pressure scheme of the same kind as the one reported by Amsden and Harlow [4], extended in the case of an implicit formulation by Braza [8] and [9], Braza et al. [7, 12]. The Navier–Stokes equations are transformed in respect to a non-orthogonal, general curvilinear coordinates system in (x,y) plan, while a Cartesian coordinate z is used for the spanwise direction. A zoom of the grid around the obstacle is shown in Figure 1. The choice ... in a previous 2D study [7], is made due to the high stability properties offered by the Douglas [13] scheme for the 3D problem. The principles of the numerical algorithm ICARE are based on the reports by Braza [10, 11]. Another useful element ...in two dimensions. The boundary conditions are those specified in Persillon and Braza [30] and are summarised in Figure 2. Concerning the spanwise free edges of the computational domain, periodic boundary conditions are applied. Etc..., etc...Therefore, by taking a spanwise length as a multiple of the simulated one and by using periodic boundary conditions, the transient phase has been considerably shortened. **Remind: First line of a new paragraph starts at 6mm**

In the following sections the results analyse the way the 3D motion is progressively installed in the flow system. The flow evolution in time and space, with emphasis to the spanwise direction, is studied by performing etc..., etc... The typical grids are of order $(250 * 100 * 80)$ to $(280 * 120 * 100)$. The parallel computers used are the IBM-SP2 of CNUSC. In the following, x is the direction along the cylinder's downstream axis, parallel to the free-stream u velocity. y is the vertical direction parallel to v velocity and z is the spanwise direction, parallel to w velocity component

Line-spacing : 15pt Leave two lines between end of paragraph and beginning of next section

2.1. ONSET OF THREE-DIMENSIONALITY (First letter 12pt, capitals, Times new Roman, 11pt)

Line-spacing : 15pt Leave one line

The present elliptic flow loses the memory of the initial conditions applied, after a transient phase whose time scale depends on the nature of the initial conditions. After detailed numerical tests in our research group [3, 32], it has been shown that the final, established stage, after the transient one is independent on the initial conditions. A special attention is devoted to ensure that *the alternating vortex shedding is extended over the whole downstream distance*, and that the wake expansion rate along x is correct, according to the physical experiment. These features have been achieved by ensuring the three following conditions: (1) A sufficiently refined grid ... around the obstacle; (2) A sufficiently large computational domain in x and y directions, ...wake expansion; (3) Adequate boundary conditions in the downstream outlet boundary, that limit the feedback effects and allow travelling the alternating eddies through this fictitious boundary without confinement (Figure 3a). Therefore, the proper development etc... the vortex shedding is limited within only one or two diameters downstream the obstacle.

After a long transient phase, needing more than 300,000 time steps during which the flow remains 2D, the w velocity component (in the spanwise direction) is progressively developed. In order to shorten this phase, a w velocity weak intensity fluctuation is applied in the inlet section ...etc... spanwise undulation. Figures 4a-4c show the progressive development of mode A in conjunction with the streamwise vortices formation. The intensity of the spanwise undulation increases from time $t=680$ to $t=740$ under the simultaneous effect of streamwise vorticity that is strengthened and forms progressively counter-clockwise 'braid' like structures (see pairs of red and yellow vortices), Figures 4a-4d.

The undulation of mode A, ...the vertical velocity component v , (Figure 5), that displays a spanwise oscillation according to a regular wavelength. The most predominant spatial mode is found 0.1171, yielding a wavelength value $\lambda_z/R=8.54$ ($\lambda_z/D=4.27$). This value is found ... announces a further fundamental modification of the spanwise structure of the main, alternating vortex rows, as it will be analysed in the next section.

2.2. THE NATURAL VORTEX DISLOCATIONS PATTERN

The instantaneous iso-vorticity fields ω_z and ω_x are first considered. During the time interval (800, 820) (Figures 4d and 4e), a noticeable change in the braid configuration of the red and yellow spanwise vortices occurs, that progressively aspirates fluid from the first violet main eddy and simultaneously this braid is displaced in a lower position. Under this effect, a clear discontinuity is obtained along the core of the second main violet vortex (Figure 4f). During these phases of the flow, mode A is also less regular.

This fundamental modification occurring on the spanwise structure of the already undulated main vortex rows *in the near wake* is called a *natural vortex dislocation*. In these intervals it can be seen that the waviness of the main vortices becomes even more fragmented along the span. It displays progressively a $2\lambda_z$ predominant wavelength, as it will be quantified in a next paragraph. The coherence of this wavelength doubling is a consequence of the perturbation caused by the passage of the vortex dislocation.

The contour plots of the vortex structures in the physical space presented in the beginning of the discussion,and wavelet analysis applied on the signals issued by the present direct simulation In the following figures, the dimensionless frequency is normalised in respect to the cylinder's radius. etc..., etc...

Therefore, by means of the present analysis, the tendency of the flow system to reduce its fundamental frequency is clearly indicated, during specific time intervals corresponding to the formation and advection of a vortex dislocation structure.

It is interesting to provide an overview of the effect of the vortex dislocations passage in a space-time map. ... This preferential structure creates the local

Strouhal number variation, associated with the passage of the vortex dislocations and with the *local frequency variation quantified by the present wavelet analysis*.

2.3. THE SPANWISE UNDULATION AS REYNOLDS NUMBER FURTHER INCREASES

At Reynolds number values higher than 220–230, ... linking the formation to the convection region (Figure 13). They pass from the lower towards the upper shear layers, by materialising well distinct vortex paths. We have performed detailed direct simulations up to the established stage, from the upper side of Reynolds number ($Re = 340$) and descending towards $Re = 230$. The Strouhal number values according to these simulations are shown in Figure 14, [3] and indicate that this mode is characterised by hysteresis and corresponds to a values-discontinuity (and not a slope discontinuity).

The present direct numerical simulation furnishes in detail the amplitude evolution *versus* period of the flow properties, as it is shown on Figure 15a, concerning the w velocity component along the rear axis of the near wake. Based on the amplitude results, it is possible to evaluate the real part of the coefficients of the Ginzburg–Landau global oscillator model:

Examples of writing equations:

$$\partial A / \partial t = \sigma_r A - I_r |A|^3 + \mu_r \partial^2 A / \partial z^2. \quad (1)$$

The term $\mu_r \partial^2 A / \partial z^2$ can also be expressed through a spanwise wavenumber, $\alpha = 2\pi / \lambda_z$ in respect to the vortex rows undulation of wavelength λ_z [23]:

$$\partial A / \partial t = \sigma_r A - I_r |A|^3 + \mu_r \alpha^2 |A|. \quad (2)$$

The first term on the right - hand side represents the linear growth, the second term corresponds to the non-linear effects before saturation and the third term represents the 3D spanwise undulation, under the form of a diffusion formulation. A is the amplitude evolution *versus* period.

The exponential growth coefficient σ_r can be written as a function of the critical Reynolds number near the threshold:

$$\sigma_r = k (Re - Re_{cr}). \quad (3)$$

According to Provansal et al. [34], k represents a reduced frequency and σ_r can be also written as:

$$\sigma_r = (1/5) (v/D^2) (Re - Re_{cr}). \quad (4)$$

where v is the cinematic viscosity and D the cylinder's radius.

If this model ... has been verified ...mode B instability is supercritical, and this has been proven in the present study by the fully non-linear approach provided by the direct simulation.

The evaluation of σ_r and l_r coefficients allows assessment of the real part of the Ginzburg–Landau coefficient, μ_r in respect to the 3D growth. In the saturation stage, the term $\partial A/\partial t$ vanishes. Therefore,

$$\mu_r = (\sigma_r - l_r A^2) / \alpha^2. \quad (5)$$

α can be evaluated by the direct simulation data for mode B, concerning λ_z , found 1.28 for Reynolds numbers (280, 300, 340). This yields an assessment of dimensionless μ_r values: ($1.3 * 10^{-3}$, $1.5 * 10^{-3}$, $2.2 * 10^{-3}$). Experimental results by Albarède and Provansal [1] provide dimensional μ_r values of order $10v$ to $40v$, that yields dimensionless values of order $0.2 * 10^{-2}$ to $5 * 10^{-2}$, for a lower Reynolds number range, and corresponding to chevron patterns due to non-parallel shedding conditions.

3. Conclusions

The present study is a continuation of our works in the domain of analysis of 3D transition in flows around bluff bodies. A detailed investigation of successive steps of transition is carried out, as Reynolds and Mach number increase. A special emphasis is devoted to the analysis of natural vortex dislocations in the low Reynolds number range.

By employing the present DNS results, the supercritical nature of this instability has been shown. This successive step of transition is able to be modelled by the Ginzburg–Landau equation, whose real-part coefficients are evaluated on the basis of the present direct simulation results.

Line-spacing : 15pt Leave two lines between end of paragraph and beginning of next section

Acknowledgements

Line-spacing : 15pt Leave one line

This work has been carried out in the research group EMT2 (Ecoulements Monophasiques, Transitionnels et Turbulents) of the Institut de Mécanique des Fluides de Toulouse. It is based on the collaborative efforts of J. Allain, A. Bouhadji, D. Faghani and H. Persillon ...computer centres of France CNUSC and IDRIS, as well of the Cornell's Supercomputing centre.

Figures can be put either in the text or at the end of the text, as in the exemple (11pts) ; (it is also possible to put two figures in the page's width)

Examples for figure captions:

Figure 1. Zoom of the grid around the body and in the near wake. (Times new Roman, 11pt)

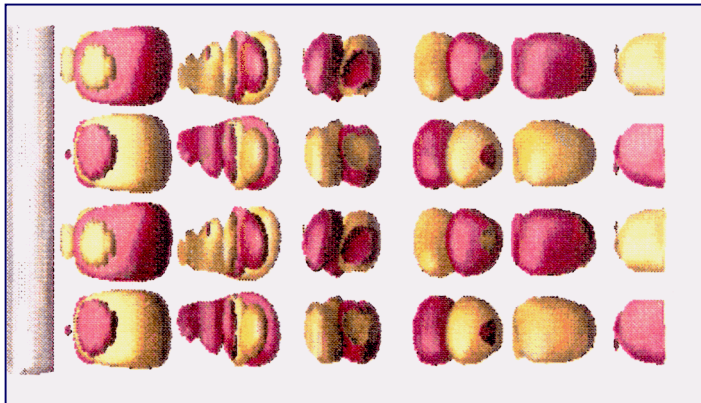
Remark: Figure captions start flush left below the figure, at 1,5 cm from the figure's frame.

Figure 2. Computational domain and boundary conditions.

Table captions are put above the Table, at 1cm from the Table's frame.

Figure 3a. Iso-vorticity contours ω_z showing persistence of the *alternating* vortex pattern over the whole computational domain

Examples for figure position and legend:



Line-spacing between Figure frame and Figure caption: 15pt.

Figure 3. (e): Development of longitudinal vorticity cells between the main eddies in the formation region. (f): Displacement of the longitudinal vortices in the shear layers, in the convection region. Same graduation as in previous figure.

Line-spacing : 15pt Leave two lines between end of paragraph and beginning of next section

References Line-spacing from: "References" up to the first line of references : 15pt.

Leave one line. Line-spacing from the first line of references up to the end: 14pt. Times New Roman 11pt

1. Albarède, P. and Provansal, M., Quasi-periodic cylinder wakes and the Ginzburg–Landau model. *J. Fluid Mech.* **291** (1995) 191–222. (Times new roman, 11pt)
2. Allain, J., Braza, M., Faghani, D. and Persillon, H., The role of natural vortex dislocations in the transition to turbulence of the flow past a circular cylinder by DNS. In: *Symposium on Direct and Large Eddy Simulations*, Eds. P. Voke, N.D. Sandham, L. Kleiser, Isaac Newton Institute for Mathematical Sciences, Publisher Kluwer, Cambridge, UK (1999) 347–357. **Examples of Journal references citation, congress proceedings and books references**
6. Bloor, M.S., Transition to turbulence in the wake of a circular cylinder. *J. Fluid Mech.* **19**, (1964), 290–304.
11. Braza, M., Analyse physique du comportement dynamique d'un écoulement externe, décollé, instationnaire, en transition laminaire-turbulente. Application: Cylindre circulaire. Thèse de Doctorat d'Etat ès Sciences, Institut National Polytechnique de Toulouse, (1986).
14. Drazin, P.G. and Reid, W.H., *Hydrodynamic Stability*, Cambridge Univ. Press, (1981).
21. Karniadakis, G.E. and Triantafyllou, G.S., Three-dimensional dynamics and transition to turbulence in the wake of bluff objects, *J. Fluid Mech.* **238** (1992) 1–30.
34. Provansal, M., Mathis, C. and Boyer, L., Bénard-von Kàrmàn instability: Transient and forced regimes. *J. Fluid Mech.* **182** (1987) 1–22.
41. Stuart, J.T., On the non-linear mechanics of wave disturbances in stable and unstable parallel flows. *J. Fluid Mech.* **9** (1960) 353–370.

6 pages maximum, including figures and references